THE JOURNAL OF PHYSICAL CHEMISTRY Letters

Letter

Cite This: J. Phys. Chem. Lett. 2019, 10, 419−426

pubs.acs.org/JPCL

Spectrally Resolved Ultrafast Exciton Transfer in Mixed Perovskite Quantum Wells

Andrew H. Proppe,[†,‡] Madeline H. Elkins,[§] Oleksandr Voznyy,[‡] Ryan D. Pensack,[§] Felipe Zapata,[∥] Lucas V. Besteiro,[⊥,#] Li Na Quan,[‡] Rafael Quintero-Bermudez,[‡] Petar Todorovic,[‡] Shana O. Kelley,[†,¶] Alexander O. Govorov,[▽] Stephen K. Gray,[○] Ivan Infante,[◆] Edward H. Sargent,*[,‡] and Gregory D. Scholes*[,§]

[†]Department of Chemistry, University of Toronto, Toronto, Ontario, Canada M5S 3G4

[‡]The Edward S. Rogers Department of Electrical and Computer Engineering, University of Toronto, Toronto, Ontario, Canada M5S 3G4

[§]Department of Chemistry, Princeton University, Princeton, New Jersey 08544, United States

[∥]Netherlands eScience Center, Science Park 140, 1098 XG Amsterdam, The Netherlands

[⊥]Institute of Fundamental and Frontier Sciences, University of Electronic Science and Technology of China, Chengdu 610054, China

[#]Centre Énergie Matériaux et Télécommunications, Institut National de la Recherche Scientifique, 1650 Boul. Lionel Boulet, Varennes, Quebec J3X 1S2, Canada

[¶]Department of Pharmaceutical Sciences, Leslie Dan Faculty of Pharmacy, University of Toronto, Toronto, Ontario, Canada M5S 3M2

[▽]Department of Physics and Astronomy, Ohio University, Athens, Ohio 45701, United States

[○]Center for Nanoscale Materials, Argonne National Laboratory, Argonne, Illinois 60439, United States

[◆]Department of Theoretical Chemistry, Faculty of Sciences, Vrije Universiteit Amsterdam, De Boelelaan 1083, 1081 HV Amsterdam, The Netherlands

Supporting Information

ABSTRACT: Solution-processed perovskite quantum wells have been used to fabricate increasingly efficient and stable optoelectronic devices. Little is known about the dynamics of photogenerated excitons in perovskite quantum wells within the first few hundred femtoseconds—a crucial time scale on which energy and charge transfer processes may compete. Here we use ultrafast transient absorption and two-dimensional electronic spectroscopy to clarify the movement of excitons and charges in reduced-dimensional perovskite solids. We report excitonic funneling from strongly to weakly confined perovskite quantum wells within 150 fs, facilitated by strong spectral overlap and orientational alignment among neighboring wells. This energy transfer happens on time scales orders of magnitude faster than charge transfer, which we find to occur instead over 10s to 100s of picoseconds. Simulations of both Förster-type interwell exciton transfer and free carrier charge transfer are in agreement with these experimental findings, with theoretical exciton transfer calculated to occur in 100s of femtoseconds.

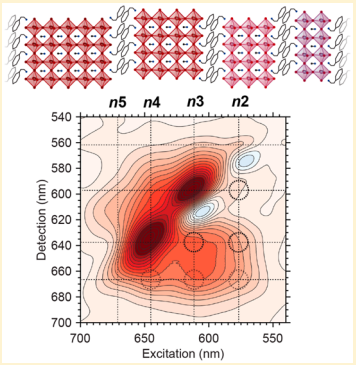

Low-dimensional perovskites are synthesized from solution by including large organic cations that form stabilized bilayer interfaces between perovskite domains.[1−3] These ligand molecules quantize the number of PbI_6^- octahedra layers between ligands (designated by an integer value, n), causing quantum and dielectric confinement along one axis, creating a quantum well (QW).[4−6] It has also been found that the resultant chemical barrier protects the lattice from degradation by water and oxygen,[4−7] increasing the device lifetime for perovskite solar cells.[8−10] At the same time, reduced-dimensional perovskite devices generally have lower power conversion efficiencies, a fact often attributed to slower charge transfer perpendicular to QWs.[5]

Previous studies have shown that exciton or free carrier transfer between QWs occurs on time scales ranging from 0.5 ps to 100s of picoseconds. Prior reports have not had the temporal resolution needed to probe <100 fs dynamics.[7,11] This picosecond transfer rate is invoked to explain improved quantum yield in light-emitting diodes made of mixed low-

Received: January 4, 2019
Accepted: January 10, 2019
Published: January 10, 2019

DOI: 10.1021/acs.jpclett.9b00018
J. Phys. Chem. Lett. 2019, 10, 419−426

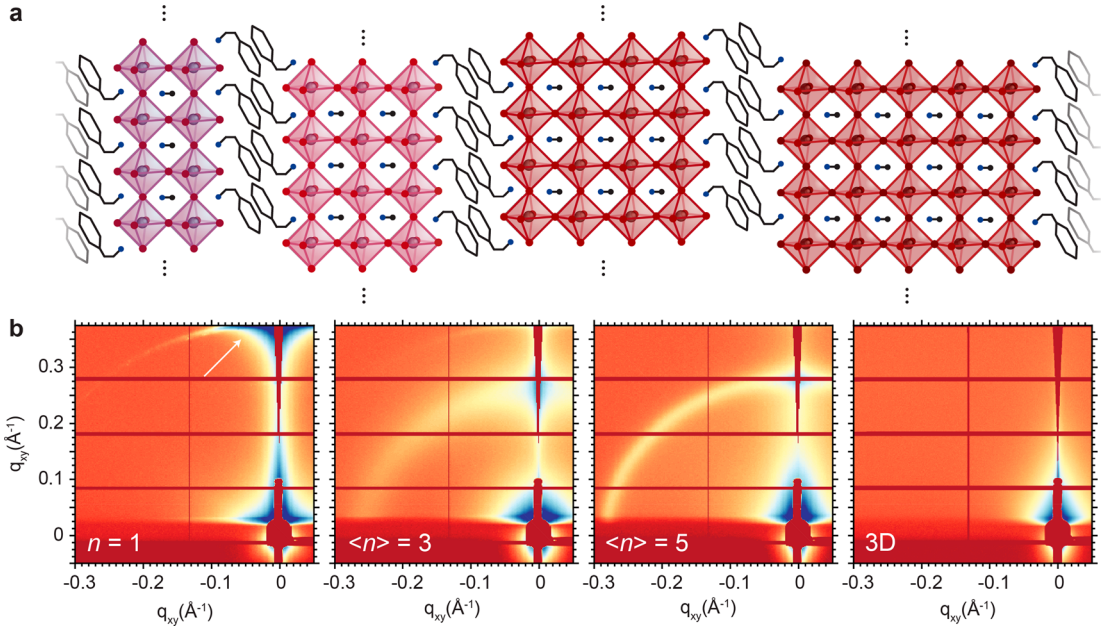

Figure 1. Molecular structure and relative orientation of perovskite quantum wells. (a) Molecular structure of *n*2, *n*3, *n*4, and *n*5 methylammonium lead halide perovskite QWs using the ligand phenethylammonium. (b) GISAXS data for thin films of pure 2D perovskite QWs ($n = 1$), $\langle n \rangle = 3$, $\langle n \rangle = 5$, and $MAPbI_3$ (3D). The anisotropic feature related to QW stacking is indicated by the white arrow. The q value of the feature is reduced with increasing n due to the increased QW thickness.

dimensional perovskites, where it is proposed that excitons undergo ultrafast energy transfer to reach lower bandgap recombination sites more effectively.[12−14] It is important to clarify the time scale on which free carrier, vs exciton, transfer occurs in reduced dimensional perovskites: light-emitting devices will benefit from ultrafast transfer and recombination of excitons, whereas light harvesting devices in contrast benefit from efficient exciton dissociation and subsequent rapid charge transfer for extraction at contacts.

To probe ultrashort time scales, we use 11 fs broadband laser pulses in transient absorption (TA) and two-dimensional electronic spectroscopy experiments. These reveal that interwell exciton transfer occurs on time scales of 100s of fs, whereas free carriers undergo charge transfer within 10s − 100s of ps. We perform simulations of both exciton transfer and free carrier charge transfer and find that the theoretically determined rates are in agreement with experimental findings.

Figure 1 illustrates the molecular structure of $n = 2-5$ QWs. The distribution of QW thicknesses within a film is governed by the central QW thickness, n, which is designated by the stoichiometry of ligand vs nonligand A-site cation molecules in the precursor solution. Due to thermodynamic mixing during the film casting, rather than QWs with only the designated thickness $\langle n \rangle$ forming, QWs of different widths centered around $\langle n \rangle$ will form instead.[6,7] For example, a choice of $\langle n \rangle \geq 3$ typically yields films that have a distribution of QWs ranging from $n = 1$ to 6+. We focus on films with two different distributions, $\langle n \rangle = 3$ and $\langle n \rangle = 5$, in order to modulate the relative populations of $n = 2-5$ QWs, whose excitonic peaks are within the bandwidth of our laser pulses.

The degree of QW size mixing affects the disorder and relative orientation of the QWs within the film, evidenced by X-ray diffraction data where both films exhibit peaks characteristic of low-*n* QWs, but the $\langle n \rangle = 5$ shows broader features associated with more randomly oriented QWs (Figure S1).[15] In order to more directly probe the orientation of the lower n QWs in our films, we used grazing-incidence small-angle X-ray scattering (GISAXS), shown in Figure 1. The strong anisotropic feature at $q_z = 3.8$ Å^{-1} in the $n = 1$ thin film indicates that the pure phase 2D QWs stack parallel to the substrate with little disorder.[15] Comparing the $\langle n \rangle = 3$ and 5 films to pure 2D and 3D films, we see that strong orientational effects persist in both types of film, meaning that a substantial population of the QWs are horizontally stacked. As the $\langle n \rangle$ value increases, we observe reduced anisotropy of the feature as it becomes more ring-like and a broadening of the peak, both of which evidence increased disorder in the orientation of the QWs. In addition, broadening of the feature suggests reduced phase purity (increased polydispersity) of the QW width distribution.

To examine ultrafast dynamics in these oriented QW films, we perform broadband TA experiments with excitation pulses that are 11 fs in duration and range from ∼550 to 700 nm. All experiments in this work were carried out at room temperature. Absorption spectra for the $\langle n \rangle = 3$ and $\langle n \rangle = 5$ films and the laser spectrum are shown in Figure 2. It can be seen that the distribution of QWs in the $\langle n \rangle = 3$ film is more tightly focused around lower n (i.e., thinner and more confined) QWs compared to $\langle n \rangle = 5$, which has significant absorption out to 750 nm, indicating the formation of quasi-3D perovskite domains in this sample. Parts a and b of Figure 2 show that both films have large amplitude negative bleach signals at early delay times for all excitonic resonances of $n = 2-6$. In $\langle n \rangle = 3$ films, we observe a rapid decay of the *n*2 and *n*3 QW signals, with a simultaneous rise in the signals for *n*4, *n*5, and *n*6+ (Figure 2a,c). In $\langle n \rangle = 5$ films, we observe instead decay of all $n < 5$ QW bleaches with a rise in the *n*6+ signal (Figure 2b,d). Time traces at the excitonic resonances and global fitting of the TA spectra reveal time constants of $\tau_1 = 170$ (300) fs, $\tau_2 = 5$ (4.5) ps, and $\tau_3 = 70$ (200) ps for the $\langle n \rangle = 3$ (5) films (see decay associated spectra, Figure S3,4). The first two time constants obtained by global fitting have a negative amplitude at the decaying QW bleaches and positive amplitude at the rising bleaches: this

DOI: 10.1021/acs.jpclett.9b00018
J. Phys. Chem. Lett. 2019, 10, 419−426

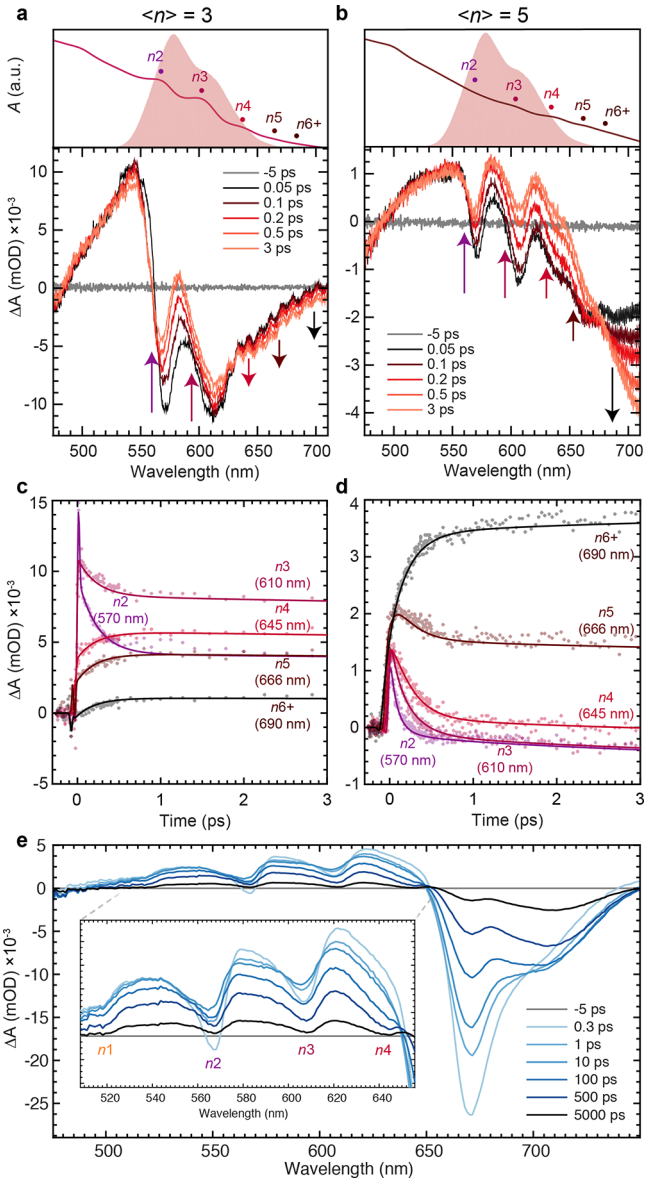

Figure 2. Broadband and narrowband transient absorption. Room temperature linear absorption spectra and spectral traces at various delay times for (a) $\langle n \rangle$ = 3 films and (b) $\langle n \rangle$ = 5 films. The laser spectrum is shown in red. The pulse duration was measured to be 11 fs (Figure S2). Excitonic peaks for different n QWs are identified according to literature references.[4,12,16] Time traces at wavelengths corresponding to QWs $n2$, $n3$, $n4$, $n5$, and $n6+$ for the (c) $\langle n \rangle$ = 3 films and (d) $\langle n \rangle$ = 5 films. Fits for time traces are obtained using global analysis.[17] (e) Narrowband transient absorption spectra of an $\langle n \rangle$ = 3 film using a photoexcitation wavelength of 670 nm (direct excitation at the exciton resonance of n = 5).

indicates population transfer from low- to high-n QWs. The third and longest globally fit time constants in both films have negative amplitude at all peaks and are consistent with carrier recombination for all QWs.[18]

We also performed narrowband TA experiments by selectively photoexciting at $n5$, below the bandgaps and exciton resonances of n = 1−4 (Figure 2e). In addition to the subpicosecond dynamics between the $n5$ QWs and the quasi-3D domains (i.e., dynamics occurring between 660−750 nm), we additionally see shifting and increasing amplitudes for the $n2$, $n3$, and $n4$ bleach signals (most obvious for $n4$) within the first 10−100s of picoseconds. In light of the reported type II band alignment between the QWs (Figure S5),[4,19,20] we assign these dynamics to holes undergoing charge transfer from the photoexcited $n \geq 5$ QWs to the lower-n wells. These rates are corroborated by similar sub-bandgap photoexcitation TA experiments on low-dimensional perovskite thin films with random[7] and graded distributions.[11]

While TA reveals an overall exchange of signal amplitudes toward higher-n QWs, it does not directly probe transitions between individual wells. Within the same QW, simultaneous rises and decays of signals (as photoexcitations move in and out of the well) are convolved. We therefore employed two-dimensional electronic spectroscopy (2DES), which correlates the excitation and detection energies into a 2D map for different population times (T_2), allowing us to spectrally resolve and isolate dynamics between the various QWs. A detailed description of this technique and our experimental setup can be found in the Methods section. 2DES spectra at various T_2 times for the $\langle n \rangle$ = 5 films are shown in Figure 3 (see Figure S6−8 for similar 2DES spectra for the $\langle n \rangle$ = 3 films). At very early T_2 times, crosspeaks between all the QW resonances within the laser bandwidth are observed, both above and below the diagonal, meaning all QWs are electronically coupled. While the on-diagonal peaks rapidly lose amplitude within the first 50 fs, the crosspeaks first gain amplitude before they too gradually decay. We note that these crosspeaks have much smaller amplitudes compared to the intense on-diagonal peaks. While the crosspeak amplitude is primarily determined by the product of the transition dipole moments, $\vec{\mu}$, between interacting QWs, here it has an additional dependence on the QW distribution, which dictates the number of instances of neighboring $n = x$ and $n = x \pm 1$ wells. Low-dimensional perovskite thin films cast at room temperature are known to form the various n QWs in a random spatial distribution as opposed to a gradient of low-to-high n,[11,15] which we confirm by photoexciting both the front and back of the thin films and obtaining identical TA signals (Figure S9). The crosspeaks indicate that these QWs may be strongly electronically coupled, and their amplitude is limited instead by the number of nearest-neighbor interactions.

We fit the on- and off-diagonal traces to biexponential functions, and the resulting time constants are shown in Table 1 (we point out wide confidence intervals from the fits owing to the limited fitting time window of 200 fs, and especially for off-diagonal peaks due to the overlapping positive and negative rates). The on-diagonal peaks all exhibit an initial <30 fs decay. This is also seen at very early delay times in the broadband TA experiments (Figure S11), but it is unaccompanied by rise times in the higher-n QW peaks, indicating this is not the result of energy or charge transfer. We attribute these initial dynamics of the on-diagonal peaks to rapid dephasing,[21,22] calculated to be ∼13−27 fs by fitting the off-diagonal fwhm (∼48−100 meV, Figure 3i and Figure S10) of the on-diagonal peaks, which gives the homogeneous line width.[23] We conclude that these rapid <30 fs dynamics are not related to charge or exciton transfer (we include a more detailed discussion of other potential origins of the <30 fs dynamics, including thermalization in quasi-3D perovskite domains[24] and the optical stark effect,[25,26] in the Supporting Discussion).

For the off-diagonal crosspeaks that contain information about ultrafast interwell dynamics, both the $n2 \rightarrow n3$ and $n2 \rightarrow n4$ crosspeaks exhibit rise times that match well within the global fits from the TA experiments. Most notably, the same rise time of ∼100 fs for the $n2 \rightarrow n3$ crosspeak is also found in the $\langle n \rangle$ = 3

DOI: 10.1021/acs.jpclett.9b00018
J. Phys. Chem. Lett. 2019, 10, 419−426

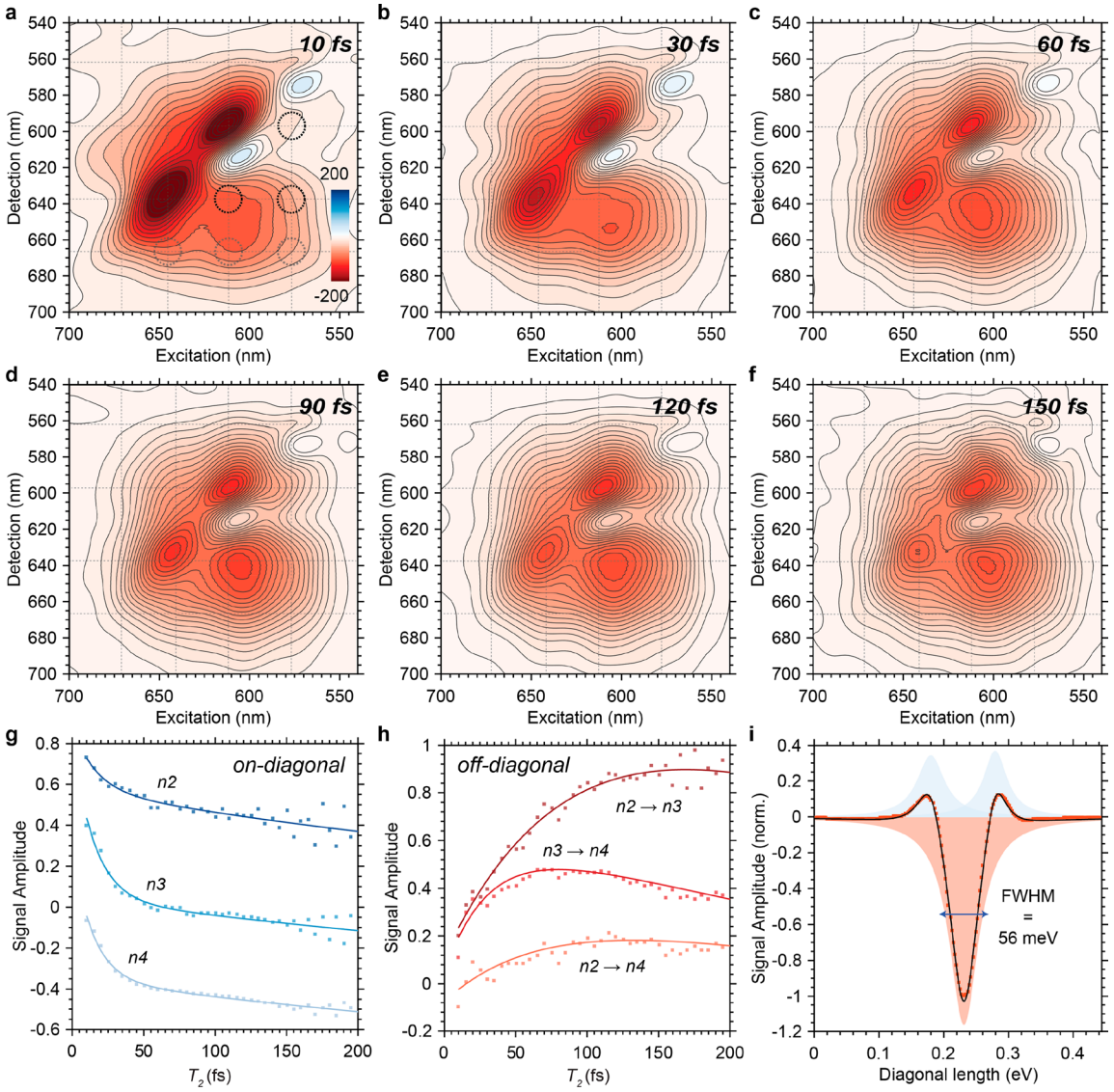

Figure 3. Two-dimensional electronic spectroscopy of $n = 5$. (a)−(f) 2DES spectra at various T_2 times. Light gray lines cross the spectra at wavelengths corresponding to the bleach maxima for QWs $n = 2$−5. Dashed circles indicate crosspeaks (darker circles are crosspeaks whose kinetic traces are in panel h). Kinetic traces extracted (g) from on-diagonal peaks for QWs $n2$, $n3$, and $n4$ throughout T_2 and (h) for off-diagonal crosspeaks occurring among the $n2$, $n3$, and $n4$ QWs. Fits and raw data are normalized and then offset for clarity. (i) Off-diagonal cut through on-diagonal $n2$ peak with fitted Lorentzians. This slice was taken from the $\langle n \rangle = 3$ film in order to get a clean estimate of the homogeneous line width. Other off-diagonal slices for $\langle n \rangle = 3$ and $\langle n \rangle = 5$ on-diagonal peaks can be found in Figure S10.

Table 1. Biexponential Fits for On- and Off-Diagonal Peaks in 2DES of $\langle n \rangle = 5$[a]

	$n2$	$n3$	$n4$	$n2 \rightarrow n3$	$n2 \rightarrow n4$	$n3 \rightarrow n4$
τ_1 (fs)	10 (±4)	26 (±10)	16 (±2)	111 (±11)*	175 (±33)*	32 (±9)*
τ_2 (fs)	390 (±100)	940 (±854)	470 (±84)	305 (±46)	385 (±49)	637 (±240)

[a]Time constants obtained from fits with 95% confidence in brackets. * indicates τ_1 times for the off-diagonal peaks correspond to positive rates (i.e., the rise times in the fitted curves) that are indicative population transfer between QWs.

films (Figure S8, Table S1), indicating that the rate of $n2 \rightarrow n3$ population transfer is the same in both films. We note that fits for low-amplitude crosspeaks (e.g., $n3 \rightarrow n4$) give positive rise times on the order of 30 fs. We attribute these extremely rapid rise times not to interwell transfer, but to strong overlap with the large amplitude on-diagonal signals: due to rapid thermalization, the on-diagonal diagonally elongated peaks rotate some of their amplitude onto the crosspeaks within the first 10s of fs (this is more evident in the sharply defined peaks in the $\langle n \rangle = 3$ films, Figure S8). We also find these 10−30 fs signals in on-diagonal and off-diagonal peaks to be unaffected by the interwell spacing (by using longer ligands), further indicating that these signals are not related to interwell transfer events (Figures S12−S14). This also suggests that another source of the <30 fs rise times at the crosspeaks could come from biexciton dephasing, manifest as a decaying excited state absorption, which we found to occur within <5−23 fs (depending on the QW size) in previous double quantum coherence spectroscopy experiments.[21]

DOI: 10.1021/acs.jpclett.9b00018
J. Phys. Chem. Lett. 2019, 10, 419−426

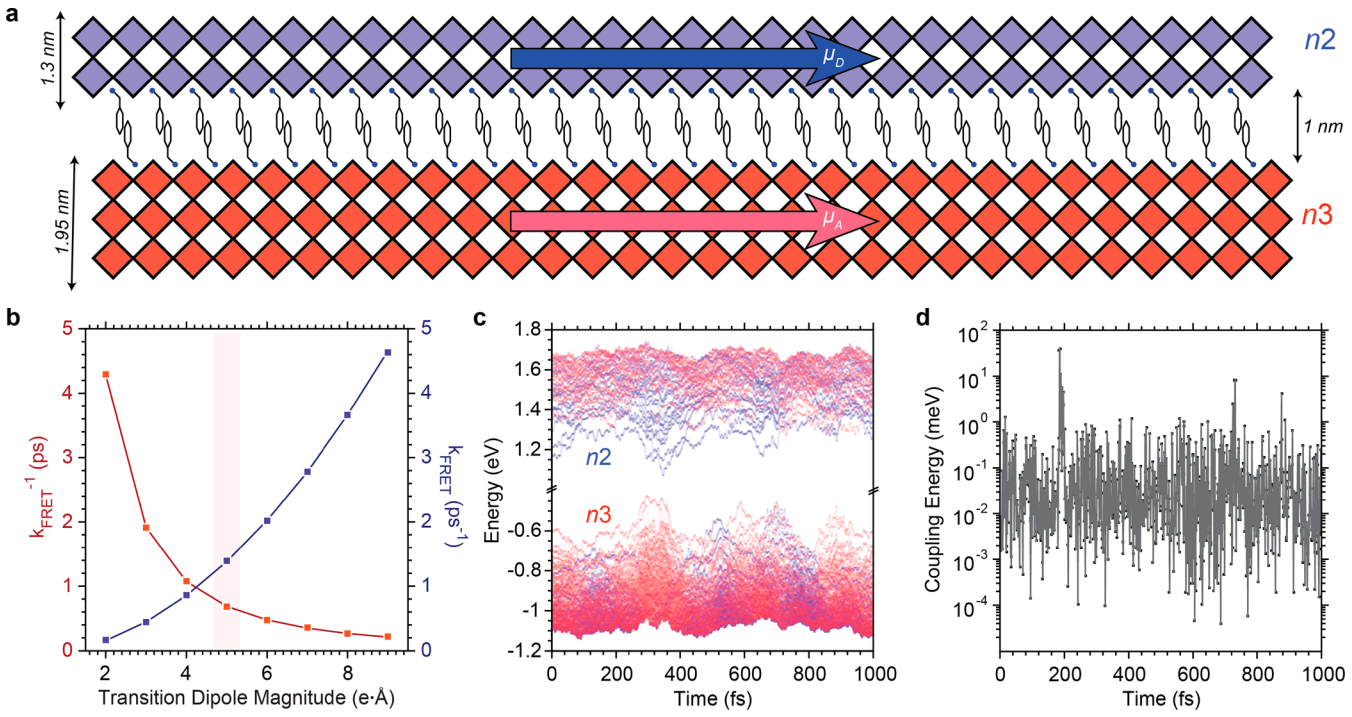

Figure 4. Calculating interwell energy transfer and charge transfer. (a) Schematic model of neighboring $n2$ and $n3$ QWs used for both FRET calculations and mixed classical-quantum dynamics calculations. Note that for FRET simulations, there is also an additional $n3$ QW above the central $n2$ donor. The interwell distance is determined from XRD (Figure S1). (b) Quadratic dependence of calculated FRET rates and energy transfer time constants on the transition dipole magnitude. (c) Time-dependent energies of numerous valence and conduction band states belonging to the $n2$ (blue) and $n3$ (red) QWs, respectively. (d) Calculated nonadiabatic couplings versus the time of the lowest $n3$ conduction band state with one of the $n2$ conduction band states that lies at similar energies and should provide an estimate of the largest interaction between the two QWs.

The 2DES experiments reveal that rapid transfer is not exclusively from low-n to much higher-n QWs but occurs also between the most highly confined QWs. Previous TA experiments on similar mixed perovskite QWs have shown population transfer from low to high n QWs occurring over a remarkably wide range of values: fully 0.3 ps to 100s of picoseconds.[11,12,19,27,28] However, the photoexcited species transferring (excitons or free carriers) has not previously been pinpointed. We believed that the disparity between reported rate constants may very well be due to an orders of magnitude difference between the rate of charge transfer of free carriers, and energy transfer of strongly bound excitons. An important consideration is that the lower-n QWs have exciton binding energies of 100s of meV,[29−31] which may preclude exciton dissociation into free carriers and subsequent charge transfer. Additionally, considering the exponential distance dependence for charge transfer, the interwell separation of 1 nm in these materials (Figure S1) would also make subpicosecond charge transfer unlikely. Our narrowband TA experiments show that holes transferring between valence bands of the various QWs occurs on much longer time scales than the dynamics found in our 2DES experiments, which also points to charge transfer being the mechanism responsible for dynamics on time scales of 10s to 100s of picoseconds.

This suggests that the mechanism behind the ultrafast interwell dynamics is exciton transfer. In the weak coupling regime, exciton transfer can described by the Förster nonradiative energy transfer (FRET) equation. FRET theories specific to QW-QW systems have been successfully used to describe energy transfer processes in inorganic GaAs QWs,[32,33] transition metal dichalcogenides,[34] and CdSe nanoplatelets.[35] The FRET rate equation

$$k = \frac{2\pi}{\hbar} |V_{DA}|^2 \int_0^\infty d\varepsilon J(\varepsilon) \quad (1)$$

contains two main elements: V_{DA}, the electronic coupling element between QWs, and J, the spectral overlap between donor and acceptor density of states. Lower-n and thus more strongly confined QWs will have larger bandgaps and blue-shifted emission, which may overlap with a higher density of states of the acceptor (higher-n) QWs. Therefore, exciton transfer rates should increase with decreasing n. This is consistent with the ultrafast global time constant in our TA experiments, which is shorter for the $\langle n \rangle$ = 3 film (170 fs) compared to the $\langle n \rangle$ = 5 film (230 fs), indicating that shifting the distribution to lower-n QWs gives rise to a faster (observed) transfer time. Furthermore, we observe increasingly faster decays with lowering-n QWs in the broadband TA experiments (Figure 2c,d).

The coupling V_{DA} between QWs might be expected to be weak owing to the relatively large interwell distance. However, for QW-QW FRET, the coupling elements have a distance dependence of d^{-4} rather than d^{-6}, owing to the extended two-dimensional interaction between the transition dipoles, and so energy transfer rates are typically enhanced in 2D systems.[32,33] V_{DA} also depends on the relative orientation of the coupled donor and acceptor transition dipole moments, $\vec{\mu}_D$ and $\vec{\mu}_A$.[36] As low-n QWs have a propensity to align parallel to each other in thin films as determined from our GISAXS experiments, this would result in $\vec{\mu}_D$ and $\vec{\mu}_A$ also being parallel, maximizing the orientation factor.[37] These very same structural properties that enhance FRET rates were found in related low-dimensional systems of stacked CdSe nanoplatelets, where extended cofacial

DOI: 10.1021/acs.jpclett.9b00018
J. Phys. Chem. Lett. 2019, 10, 419−426

contact between platelets lead to stronger donor−acceptor coupling and enhanced exciton transfer rates.[35]

A theoretical estimate of the interwell $n2$ to $n3$ FRET rate can also be found with same model that was successfully employed for these CdSe nanoplatelets systems,[35] which takes the rate to be (SI units)

$$k_{\mathrm{FRET}} = \frac{2}{\hbar}\epsilon_0 \,\mathrm{Im}[\epsilon_{\mathrm{A}}(\omega_{\mathrm{emitter}})] \int_{\mathrm{A}} |\mathbf{E}|^2 \,\mathrm{d}V \tag{2}$$

where ϵ_0 is the permittivity of free space, the electric field $\mathbf{E}$ results from assuming the donor is described by a classical donor dipole oriented as indicated in Figure 4a, and ϵ_{A} is the acceptor relative dielectric constant. We take donor ($n2$) and acceptor ($n3$) units to be stacked face-to-face with square facial dimensions of 50 nm × 50 nm and separations and thicknesses as indicated in Figure 4a. The volume integral is taken over acceptor units, stacked both above and below a donor. We assume donor dipole strengths are in the range $\mu_{\mathrm{D}} = e{\cdot}5$ Å on the basis of monolayer absorption spectra, and from the observation that these perovskite QWs have oscillator strengths more than 2 orders of magnitude larger than inorganic GaAs QWs, and also more than twice as strong as transition metal dichalcogenides.[38] We take the molecular interface region between donor and acceptors to have a dielectric constant of 2.38 (toluene). For simplicity we assume the dielectric constants for $n2$ and $n3$ are similar and, for the donor emitter wavelength ($\frac{2\pi c}{\omega_{\mathrm{emitter}}} = 570$ nm), we have $\epsilon_{\mathrm{A}} = \epsilon_{\mathrm{D}} = 5.6 + 1.9\mathrm{i}$ (extracted from ellipsometry measurements on $MAPbI_3$).[39] The electric field $\mathbf{E}$ is estimated with full COMSOL electrodynamics calculations identical to those of ref 35. We obtain $k_{\mathrm{FRET}} = 1.46\ \mathrm{ps}^{-1}$, corresponding to an energy transfer time constant of 0.687 ps, matching closely with our experimental results. From eq 2, we see that this energy transfer rate varies quadratically with the magnitude of the transition dipole moment (Figure 4b) and also increases with decreasing interwell distance (Figure S16). For all values of μ_{D} greater than $\sim e{\cdot}4$ Å, subpicosecond energy transfer rates are obtained. While the interwell distances may exhibit small fluctuations that could lead to slightly faster energy transfer, it is possible that the transition dipole moment used in these calculations may be even larger than we estimate here, in light of the exceptionally large oscillator strengths of these materials.[38,40] This would lead to even faster energy transfer rates that approach our experimentally measured dynamics.

While our theoretical FRET rates match well with the interwell dynamics measured by 2DES, we also sought to evaluate whether these QWs have sufficiently strong coupling between free carrier states that could lead to ultrafast interwell charge transfer. We thus performed mixed classical-quantum dynamics combined with the fewest-switches surface hopping algorithm, where the quantum chemical problem was solved by carrying out atomistic ab initio molecular dynamics (AIMD) simulations at the density functional theory (DFT) level of theory using the Perdew−Burke−Ernzerhof exchange−correlation functional[41] and a canonical ensemble at 300 K (Figure 4). The time-dependent electronic structure of the combined $n2$−$n3$ system (Figure 4c) shows QW orbital energies continuously fluctuating out-of-phase, preventing a clear-cut orbital energy alignment between the two QWs. Such out-of-phase oscillations could already indicate strong decoherence, and thus a first indication of a hindered charge transfer process. We then employed the surface hopping algorithm by stochastically realizing 1000 trajectories to reconstruct the quantum probabilities. The resulting nonadiabatic couplings from one such trajectory are shown in Figure 4d. We see that these couplings never exceed values higher than ∼40 meV, suggesting that charge transfer between these QWs will proceed very slowly. In order to construct time-dependent population dynamics, we populate either the $n2$ (3) electron or holes at the beginning of each trajectory and follow their population over time, which we observe in all cases to be constant within our time window (Figures S17 and S18), again indicating that the charge transfer process is very slow. As a further assessment of these results, we have grouped together all states belonging to each QW and we observed if there was any flux of carrier transport between the wells. Also in this case we see that the population transfer is negligible in the time scale considered (Figure S19), indicating that the process occurs at on time scales longer than 1 ps. This result supports our conclusion that interwell exciton transfer proceeds on time scales of 100s of fs, whereas time scales for charge transfer extend far beyond 1 ps.

By probing dynamics at ultrashort times following photogeneration of excitons, we have been able to identify the time scales for energy and charge transfer of excitons and free carriers in mixed perovskite QWs. We have demonstrated that exciton transfer occurs on a time scale of 100s of femtoseconds between all perovskite QWs, whereas free carriers undergo charge transfer instead on a 1−100 ps time scale. In natural light harvesting systems like photosystem supercomplexes,[42] ultrafast electronic energy transfer of Frenkel excitons[43] initially occurs between closely packed pigments within proteins,[44] whereas subsequent migration of these photoexcitations over distances of 10s of nanometers occurs through multiple hopping steps.[45,46] We find here that electronic energy transfer across comparable nanoscale distances occurs on much faster time scales. The theoretical studies support the view that this arises due to delocalization of photoexcitations across laterally wide QWs that are well oriented in solid state.

The ability to direct such remarkably fast electronic energy transfer has important implications for perovskite QW optoelectronic devices. In light emitting devices, extremely fast energy transfer is desirable, especially with higher carrier densities, to outpace Auger recombination,[35,47] charge transfer, and trapping in order to preserve and funnel excitons to lower bandgap QWs either for individual recombination events that increase the quantum yield for LEDs[12,27,48] or for the accumulation of multiple excitons at acceptor wells that benefits lasing. For light harvesting devices, ultrafast exciton funneling directs the more strongly bound excitons toward less confined QWs, where, instead of promoting recombination, they can facilitate dissociation of excitons into free carriers[16,49] which then undergo multiple charge transfer events over several nanoseconds[11] to electrical contacts in order to generate photocurrent. These findings add to models of photoinduced dynamics in mixed perovskite QWs relevant to the design and optimization of future devices.

■ ASSOCIATED CONTENT

Supporting Information

The Supporting Information is available free of charge on the ACS Publications website at DOI: 10.1021/acs.jpclett.9b00018.

Materials and methods; XRD, laser pulse profile, time constants and residuals, UPS data, 2DES spectra, on- and off-diagonal time traces, front and back photoexcitation of film, off-diagonal cuts through on-diagonal peaks, TA

DOI: 10.1021/acs.jpclett.9b00018
J. Phys. Chem. Lett. 2019, 10, 419−426

experiments and fluence dependence, optical Stark effect in low-*n* perovskite QWs, FRET rate constants, orbital energies and band-gap energies, population transfer via charge transfer, and population vs time (Figures S1–S19); table of biexponential fits for on- and off-diagonal time traces; discussion of and the optical Stark effect, Forster resonance energy transfer simulation details, and nonadiabatic molecular dynamics (PDF)

AUTHOR INFORMATION

Corresponding Authors

*Edward H. Sargent. E-mail: ted.sargent@utoronto.ca.
*Gregory D. Scholes. E-mail: gscholes@princeton.edu.

ORCID

Andrew H. Proppe: 0000-0003-3860-9949
Madeline H. Elkins: 0000-0001-5076-8577
Oleksandr Voznyy: 0000-0002-8656-5074
Ryan D. Pensack: 0000-0002-1302-1770
Lucas V. Besteiro: 0000-0001-7356-7719
Li Na Quan: 0000-0001-9301-3764
Rafael Quintero-Bermudez: 0000-0002-4233-395X
Shana O. Kelley: 0000-0003-3360-5359
Alexander O. Govorov: 0000-0003-1316-6758
Ivan Infante: 0000-0003-3467-9376
Edward H. Sargent: 0000-0003-0396-6495
Gregory D. Scholes: 0000-0003-3336-7960

Notes

The authors declare no competing financial interest.

ACKNOWLEDGMENTS

M.H.E., E.H.S., and G.D.S. gratefully acknowledge the support of the Canadian Institute for Advanced Research through its Bioinspired Solar Energy program. Additionally, E.H.S. acknowledges the Ontario Fund: Research Excellence Program, the Natural Sciences and Engineering Research Council of Canada, and a University of Toronto Connaught grant. G.D.S. thanks Princeton University through the Innovation Fund for New Ideas in the Natural Sciences. I.I. acknowledges The Netherlands Organization of Scientific Research (NWO) for financial support through the Innovational Research Incentive (Vidi) Scheme (Grant No. 723.013.002). The AIMS simulations were carried out on the Dutch national e-infrastructure with the support of the SURF Cooperative. This work was performed, in part, at the Center for Nanoscale Materials, a U.S. Department of Energy Office of Science User Facility, and supported by the U.S. Department of Energy, Office of Science, under Contract No. DE-AC02-06CH11357. A.H.P. is supported by the Fonds de Recherche du Québec- Nature et Technologies and the Ontario Graduate Scholarship program. We thank A. Jain, M. Korkusinsk,I and A. Aspuru-Guzik for fruitful discussions.

REFERENCES

(1) Weidman, M. C.; Seitz, M.; Stranks, S. D.; Tisdale, W. A. Highly Tunable Colloidal Perovskite Nanoplatelets through Variable Cation, Metal, and Halide Composition. *ACS Nano* **2016**, *10*, 7830–7839.

(2) Sichert, J. A.; Tong, Y.; Mutz, N.; Vollmer, M.; Fischer, S.; Milowska, K. Z.; García Cortadella, R.; Nickel, B.; Cardenas-Daw, C.; Stolarczyk, J. K.; Urban, A. S.; Feldmann, J. Quantum Size Effect in Organometal Halide Perovskite Nanoplatelets. *Nano Lett.* **2015**, *15*, 6521–6527.

(3) Tyagi, P.; Arveson, S. M.; Tisdale, W. A. Colloidal Organohalide Perovskite Nanoplatelets Exhibiting Quantum Confinement. *J. Phys. Chem. Lett.* **2015**, *6*, 1911–1916.

(4) Cao, D. H.; Stoumpos, C. C.; Farha, O. K.; Hupp, J. T.; Kanatzidis, M. G. 2D Homologous Perovskites as Light-Absorbing Materials for Solar Cell Applications. *J. Am. Chem. Soc.* **2015**, *137*, 7843–7850.

(5) Tsai, H.; Nie, W.; Blancon, J.-C.; Stoumpos, C. C.; Asadpour, R.; Harutyunyan, B.; Neukirch, A. J.; Verduzco, R.; Crochet, J. J.; Tretiak, S.; Pedesseau, L.; Even, J.; Alam, M. A.; Gupta, G.; Lou, J.; Ajayan, P. M.; Bedzyk, M. J.; Kanatzidis, M. G.; Mohite, A. D. High-Efficiency Two-Dimensional Ruddlesden–Popper Perovskite Solar Cells. *Nature* **2016**, *536*, 312–316.

(6) Quan, L. N.; Yuan, M.; Comin, R.; Voznyy, O.; Beauregard, E. M.; Hoogland, S.; Buin, A.; Kirmani, A. R.; Zhao, K.; Amassian, A.; Kim, D. H.; Sargent, E. H. Ligand-Stabilized Reduced-Dimensionality Perovskites. *J. Am. Chem. Soc.* **2016**, *138*, 2649–2655.

(7) Proppe, A. H.; Quintero-Bermudez, R.; Tan, H.; Voznyy, O.; Kelley, S. O.; Sargent, E. H. Synthetic Control over Quantum Well Width Distribution and Carrier Migration in Low-Dimensional Perovskite Photovoltaics. *J. Am. Chem. Soc.* **2018**, *140*, 2890–2896.

(8) Grancini, G.; Roldán-Carmona, C.; Zimmermann, I.; Mosconi, E.; Lee, X.; Martineau, D.; Narbey, S.; Oswald, F.; De Angelis, F.; Graetzel, M.; Nazeeruddin, M. K. One-Year Stable Perovskite Solar Cells by 2D/3D Interface Engineering. *Nat. Commun.* **2017**, *8*, 15684.

(9) Cho, K. T.; Grancini, G.; Lee, Y.; Oveisi, E.; Ryu, J.; Almora, O.; Tschumi, M.; Schouwink, P. A.; Seo, G.; Heo, S.; Park, J.; Jang, J.; Paek, S.; Garcia-Belmonte, G.; Nazeeruddin, M. K. Selective Growth of Layered Perovskites for Stable and Efficient Photovoltaics. *Energy Environ. Sci.* **2018**, *11*, 952–959.

(10) Wang, Z.; Lin, Q.; Chmiel, F. P.; Sakai, N.; Herz, L. M.; Snaith, H. J. Efficient Ambient-Air-Stable Solar Cells with 2D–3D Heterostructured Butylammonium-Caesium-Formamidinium Lead Halide Perovskites. *Nat. Energy* **2017**, *2*, 17135.

(11) Liu, J.; Leng, J.; Wu, K.; Zhang, J.; Jin, S. Observation of Internal Photoinduced Electron and Hole Separation in Hybrid Two-Dimensional Perovskite Films. *J. Am. Chem. Soc.* **2017**, *139*, 1432–1435.

(12) Yuan, M.; Quan, L. N.; Comin, R.; Walters, G.; Sabatini, R.; Voznyy, O.; Hoogland, S.; Zhao, Y.; Beauregard, E. M.; Kanjanaboos, P.; Lu, Z.; Kim, D. H.; Sargent, E. H. Perovskite Energy Funnels for Efficient Light-Emitting Diodes. *Nat. Nanotechnol.* **2016**, *11*, 872–877.

(13) Byun, J.; Cho, H.; Wolf, C.; Jang, M.; Sadhanala, A.; Friend, R. H.; Yang, H.; Lee, T.-W. Efficient Visible Quasi-2D Perovskite Light-Emitting Diodes. *Adv. Mater.* **2016**, *28*, 7515–7520.

(14) Li, M.; Gao, Q.; Liu, P.; Liao, Q.; Zhang, H.; Yao, J.; Hu, W.; Wu, Y.; Fu, H. Amplified Spontaneous Emission Based on 2D Ruddlesden–Popper Perovskites. *Adv. Funct. Mater.* **2018**, *28*, 1707006.

(15) Quintero-Bermudez, R.; Gold-Parker, A.; Proppe, A. H.; Munir, R.; Yang, Z.; Kelley, S. O.; Amassian, A.; Toney, M. F.; Sargent, E. H. Compositional and Orientational Control in Metal Halide Perovskites of Reduced Dimensionality. *Nat. Mater.* **2018**, *17*, 900.

(16) Wu, X.; Trinh, M. T.; Zhu, X.-Y. Excitonic Many-Body Interactions in Two-Dimensional Lead Iodide Perovskite Quantum Wells. *J. Phys. Chem. C* **2015**, *119*, 14714–14721.

(17) Snellenburg, J. J.; Laptenok, S.; Seger, R.; Mullen, K. M.; Stokkum, I. H. M. van Glotaran: A Java-Based Graphical User Interface for the R Package TIMP. *J. Stat. Softw.* **2012**, *49*, 1–22.

(18) Yamada, Y.; Nakamura, T.; Endo, M.; Wakamiya, A.; Kanemitsu, Y. Photocarrier Recombination Dynamics in Perovskite CH3NH3PbI3 for Solar Cell Applications. *J. Am. Chem. Soc.* **2014**, *136*, 11610–11613.

(19) Shang, Q.; Wang, Y.; Zhong, Y.; Mi, Y.; Qin, L.; Zhao, Y.; Qiu, X.; Liu, X.; Zhang, Q. Unveiling Structurally Engineered Carrier Dynamics in Hybrid Quasi-Two-Dimensional Perovskite Thin Films toward Controllable Emission. *J. Phys. Chem. Lett.* **2017**, *8*, 4431–4438.

(20) Safdari, M.; Svensson, P. H.; Hoang, M. T.; Oh, I.; Kloo, L.; Gardner, J. M. Layered 2D Alkyldiammonium Lead Iodide Perovskites: Synthesis, Characterization, and Use in Solar Cells. *J. Mater. Chem. A* **2016**, *4*, 15638–15646.

(21) Elkins, M. H.; Pensack, R.; Proppe, A. H.; Voznyy, O.; Quan, L. N.; Kelley, S. O.; Sargent, E. H.; Scholes, G. D. Biexciton Resonances

DOI: 10.1021/acs.jpclett.9b00018
J. Phys. Chem. Lett. 2019, 10, 419–426

Reveal Exciton Localization in Stacked Perovskite Quantum Wells. *J. Phys. Chem. Lett.* **2017**, *8*, 3895−3901.
(22) Duan, H.-G.; Prokhorenko, V. I.; Cogdell, R. J.; Ashraf, K.; Stevens, A. L.; Thorwart, M.; Miller, R. J. D. Nature Does Not Rely on Long-Lived Electronic Quantum Coherence for Photosynthetic Energy Transfer. *Proc. Natl. Acad. Sci. U. S. A.* **2017**, *114*, 8493−8498.
(23) Moody, G.; Kavir Dass, C.; Hao, K.; Chen, C.-H.; Li, L.-J.; Singh, A.; Tran, K.; Clark, G.; Xu, X.; Berghäuser, G.; Malic, E.; Knorr, A.; Li, X. Intrinsic Homogeneous Linewidth and Broadening Mechanisms of Excitons in Monolayer Transition Metal Dichalcogenides. *Nat. Commun.* **2015**, *6*, 8315.
(24) Richter, J. M.; Branchi, F.; Valduga de Almeida Camargo, F.; Zhao, B.; Friend, R. H.; Cerullo, G.; Deschler, F. Ultrafast Carrier Thermalization in Lead Iodide Perovskite Probed with Two-Dimensional Electronic Spectroscopy. *Nat. Commun.* **2017**, *8*, 376.
(25) Giovanni, D.; Chong, W. K.; Dewi, H. A.; Thirumal, K.; Neogi, I.; Ramesh, R.; Mhaisalkar, S.; Mathews, N.; Sum, T. C. Tunable Room-Temperature Spin-Selective Optical Stark Effect in Solution-Processed Layered Halide Perovskites. *Sci. Adv.* **2016**, *2*, e1600477.
(26) Yang, Y.; Yang, M.; Zhu, K.; Johnson, J. C.; Berry, J. J.; van de Lagemaat, J.; Beard, M. C. Large Polarization-Dependent Exciton Optical Stark Effect in Lead Iodide Perovskites. *Nat. Commun.* **2016**, *7*, 12613.
(27) Wang, N.; Cheng, L.; Ge, R.; Zhang, S.; Miao, Y.; Zou, W.; Yi, C.; Sun, Y.; Cao, Y.; Yang, R.; Wei, Y.; Guo, Q.; Ke, Y.; Yu, M.; Jin, Y.; Liu, Y.; Ding, Q.; Di, D.; Yang, L.; Xing, G.; et al. Perovskite Light-Emitting Diodes Based on Solution-Processed Self-Organized Multiple Quantum Wells. *Nat. Photonics* **2016**, *10*, 699−704.
(28) Xing, G.; Wu, B.; Wu, X.; Li, M.; Du, B.; Wei, Q.; Guo, J.; Yeow, E. K. L.; Sum, T. C.; Huang, W. Transcending the Slow Bimolecular Recombination in Lead-Halide Perovskites for Electroluminescence. *Nat. Commun.* **2017**, *8*, 14558.
(29) Hong, X.; Ishihara, T.; Nurmikko, A. V. Dielectric Confinement Effect on Excitons in PbI4-Based Layered Semiconductors. *Phys. Rev. B: Condens. Matter Mater. Phys.* **1992**, *45*, 6961−6964.
(30) Ishihara, T.; Takahashi, J.; Goto, T. Exciton State in Two-Dimensional Perovskite Semiconductor (C10H21NH3)2PbI4. *Solid State Commun.* **1989**, *69*, 933−936.
(31) Ishihara, T.; Takahashi, J.; Goto, T. Optical Properties Due to Electronic Transitions in Two-Dimensional Semiconductors (CnH2n+1NH3)2PbI4. *Phys. Rev. B: Condens. Matter Mater. Phys.* **1990**, *42*, 11099−11107.
(32) Tomita, A.; Shah, J.; Knox, R. S. Efficient Exciton Energy Transfer between Widely Separated Quantum Wells at Low Temperatures. *Phys. Rev. B: Condens. Matter Mater. Phys.* **1996**, *53*, 10793−10803.
(33) Lyo, S. K. Energy Transfer of Excitons between Quantum Wells Separated by a Wide Barrier. *Phys. Rev. B: Condens. Matter Mater. Phys.* **2000**, *62*, 13641−13656.
(34) Kozawa, D.; Carvalho, A.; Verzhbitskiy, I.; Giustiniano, F.; Miyauchi, Y.; Mouri, S.; Castro Neto, A. H.; Matsuda, K.; Eda, G. Evidence for Fast Interlayer Energy Transfer in MoSe2/WS2 Heterostructures. *Nano Lett.* **2016**, *16*, 4087−4093.
(35) Rowland, C. E.; Fedin, I.; Zhang, H.; Gray, S. K.; Govorov, A. O.; Talapin, D. V.; Schaller, R. D. Picosecond Energy Transfer and Multiexciton Transfer Outpaces Auger Recombination in Binary CdSe Nanoplatelet Solids. *Nat. Mater.* **2015**, *14*, 484−489.
(36) Beljonne, D.; Curutchet, C.; Scholes, G. D.; Silbey, R. J. Beyond Förster Resonance Energy Transfer in Biological and Nanoscale Systems. *J. Phys. Chem. B* **2009**, *113*, 6583−6599.
(37) Scholes, G. D. Long-Range Resonance Energy Transfer in Molecular Systems. *Annu. Rev. Phys. Chem.* **2003**, *54*, 57−87.
(38) Yaffe, O.; Chernikov, A.; Norman, Z. M.; Zhong, Y.; Velauthapillai, A.; van der Zande, A.; Owen, J. S.; Heinz, T. F. Excitons in Ultrathin Organic-Inorganic Perovskite Crystals. *Phys. Rev. B: Condens. Matter Mater. Phys.* **2015**, *92*, 045414.
(39) Phillips, L. J.; Rashed, A. M.; Treharne, R. E.; Kay, J.; Yates, P.; Mitrovic, I. Z.; Weerakkody, A.; Hall, S.; Durose, K. Dispersion Relation Data for Methylammonium Lead Triiodide Perovskite Deposited on a (100) Silicon Wafer Using a Two-Step Vapour-Phase Reaction Process. *Data Brief* **2015**, *5*, 926−928.
(40) Zhang, Q.; Chu, L.; Zhou, F.; Ji, W.; Eda, G. Excitonic Properties of Chemically Synthesized 2D Organic-Inorganic Hybrid Perovskite Nanosheets. *Adv. Mater.* **2018**, *30*, 1704055.
(41) Perdew, J. P.; Burke, K.; Ernzerhof, M. Generalized Gradient Approximation Made Simple. *Phys. Rev. Lett.* **1996**, *77*, 3865−3868.
(42) Scholes, G. D.; Fleming, G. R.; Olaya-Castro, A.; van Grondelle, R. Lessons from Nature about Solar Light Harvesting. *Nat. Chem.* **2011**, *3*, 763−774.
(43) Scholes, G. D.; Rumbles, G. Excitons in Nanoscale Systems. *Nat. Mater.* **2006**, *5*, 683−696.
(44) Wendling, M.; Mourik, F. van; Stokkum, I. H. M. van; Salverda, J. M.; Michel, H.; Grondelle, R. van. Low-Intensity Pump-Probe Measurements on the B800 Band of Rhodospirillum Molischianum. *Biophys. J.* **2003**, *84*, 440−449.
(45) van Grondelle, R.; Bergström, H.; Sundström, V.; Gillbro, T. Energy Transfer within the Bacteriochlorophyll Antenna of Purple Bacteria at 77 K, Studied by Picosecond Absorption Recovery. *Biochim. Biophys. Acta, Bioenerg.* **1987**, *894*, 313−326.
(46) Ma, Y.-Z.; Cogdell, R. J.; Gillbro, T. Energy Transfer and Exciton Annihilation in the B800−850 Antenna Complex of the Photosynthetic Purple Bacterium Rhodopseudomonas Acidophila (Strain 10050). A Femtosecond Transient Absorption Study. *J. Phys. Chem. B* **1997**, *101*, 1087−1095.
(47) Aneesh, J.; Swarnkar, A.; Kumar Ravi, V.; Sharma, R.; Nag, A.; Adarsh, K. V. Ultrafast Exciton Dynamics in Colloidal CsPbBr3 Perovskite Nanocrystals: Biexciton Effect and Auger Recombination. *J. Phys. Chem. C* **2017**, *121*, 4734−4739.
(48) Hu, H.; Salim, T.; Chen, B.; Lam, Y. M. Molecularly Engineered Organic-Inorganic Hybrid Perovskite with Multiple Quantum Well Structure for Multicolored Light-Emitting Diodes. *Sci. Rep.* **2016**, *6*, 33546.
(49) Jha, A.; Duan, H.-G.; Tiwari, V.; Nayak, P. K.; Snaith, H. J.; Thorwart, M.; Miller, R. J. D. Direct Observation of Ultrafast Exciton Dissociation in Lead Iodide Perovskite by 2D Electronic Spectroscopy. *ACS Photonics* **2018**, *5*, 852−860.

DOI: 10.1021/acs.jpclett.9b00018
J. Phys. Chem. Lett. 2019, 10, 419−426